We are IntechOpen, the world's leading publisher of Open Access books Built by scientists, for scientists

4,800
Open access books available

122,000
International authors and editors

135M
Downloads

Our authors are among the

154
Countries delivered to

TOP 1%
most cited scientists

12.2%
Contributors from top 500 universities

CLARIVATE ANALYTICS BOOK CITATION INDEX INDEXED

WEB OF SCIENCE™

Selection of our books indexed in the Book Citation Index in Web of Science™ Core Collection (BKCI)

Interested in publishing with us?
Contact book.department@intechopen.com

Numbers displayed above are based on latest data collected.
For more information visit www.intechopen.com

21

Study on Three Dimensional Dual Peg-in-hole in Robot Automatic Assembly

Fei Yanqiong[1], Wan Jianfeng[2], Zhao Xifang[1]
[1]*Research Institute of Robotics,*
Shanghai Jiao Tong University,
Huashan Road 1954, Shanghai 200030 (P. R. of China)
[2]*School of Materials Science and Engineering,*
Shanghai Jiao Tong University,
Huashan Road 1954, Shanghai 200030 (P. R. of China)

1. Introduction and Importance

The analyses of the physics of robot assembly tasks are important in developing a flexible assembly system. Assembly analyses involve force/moment analysis due to contacts and jamming analysis due to improper force/moment.

Because the uncertainty of geometry and control, contact states exist during the assembly process. Xiao presented the notion of contact formation (CF) in terms of principal contacts (PCs) to characterize contact states, and defined contact states as CF-connected regions of contact configurations (Xiao, 1993). They also examined the neighboring relations between contact states and characterized the contact state space as a contact state graph. Xiao developed an algorithm that automatically generated a high-level contact state graph and planned contact motions between two known adjacent contact states (Xiao, 2001).

Force/moment analysis is an important element in robot assembly analyses. Lots of research has been done on single peg-in-hole. Simunivic analyzed a round peg insertion problem, and derived two dimensional single peg-in-hole jamming conditions (Simunivic, 1972). Whitney adopted Simunovic's approach to determine the force analysis of the same problem (Whitney, 1982). He identified wedging and jamming conditions and recommended ways to avoid insertion failure. A compliant mechanism, RCC (Remote-Center-Compliance) was designed for axisymmetric part insertions. Sturges and Laowattana analyzed the wedging condition in rectangular peg insertion and developed a Spatial Remote-Center-Compliance (SRCC) (Sturges, 1988, 1996, 1996). Non-axisymmetric part insertions can be performed. Tsaprounis focused on the determination of forces at contact points between a round peg and a hole (Tsaprounis, 1998).

Considerable theories have also been studied over the past years that define two dimensional mating between double rigid cylindrical parts (Arai, 1997, McCarragher, 1995 and Sathirakul, 1998). Arai described error models and analyzed the search strategy of a two dimensional dual peg-in-hole (Arai, 1997). McCarragher modeled assembly as a discrete event dynamic system using Petri nets and developed a discrete event controller

Source: Industrial Robotics: Programming, Simulation and Applicationl, ISBN 3-86611-286-6, pp. 702, ARS/plV, Germany, December 2006, Edited by: Low Kin Huat

(McCarragher, 1995). He applied his method to a two dimensional dual peg-in-hole insertion successfully. Sturges analyzed two dimensional dual peg-in-hole insertion problems, enumerated possible contact states, and derived geometric conditions and force-moment equations for static-equilibrium states of two dimensional dual peg insertions (Sathirakul and Sturges, 1998). The jamming diagrams of a two dimensional dual peg-in-hole were obtained.

At present, research activities in the area are concentrated on:

(1) Three dimensional multiple peg-in-hole analyses
(2) Modeling of contact
(3) Design of assembly devices

Multiple peg-in-hole insertions represent a class of practical and complicated tasks in the field of robotic automatic assembly. Because of the difficulty and complexity in analyzing three dimensional multiple peg-in-hole insertions, most of the analyses of this class of assembly tasks to date were done by simplifying the problems into two dimensions (Arai, 1997, McCarragher, 1995 and Sathirakul, 1998). The analyses of the dual peg-in-hole in three dimensions are few (Rossitza, 1998). Rossitza considered the geometric model and quasi-static force model of a three dimensional dual peg-in-hole and presented a method for 3D simulation of the dual peg insertion. The assembly process, considered as a sequence of discrete contact events, is modeled as a transition from one state to another. Sturges' work on the three dimensional analysis of multiple-peg insertion gave insight into the behavior of the pegs during the chamfer-crossing phase of the problem (Sturges, 1996). The net forces and torque during chamfer-crossing of a triple-peg insertion were obtained. The force/torque prediction gave a better insight into the physics of multiple peg-in-hole insertion with the aid of compliance mechanisms (SRCC) (Sturges, 1996). Fei's geometric analysis of a triple peg-in-hole mechanism gives the base of three dimensional assembly problems (Fei, 2003). The geometric features of three-dimensional assembly objects are represented by two elements. The geometric conditions for each contact state are derived with the transformation matrix (Fei, 2003).

However, for three dimensional multiple peg-in-hole insertion tasks, there are not yet perfect assembly theory and experimental analyses at present. After analyzing multiple peg-in-hole in three dimensions, the whole assembly process and its complexity and difficulty can be known in detail. Thus, some simple and special machines can be designed to finish this type of tasks.

In the paper, a complete contact and jamming analysis of dual peg-in-hole insertion is described in three dimensions. By understanding the physics of three dimensional assembly processes, one can plan fine motion strategies and guarantee successful operations.

In this article, three dimensional dual peg-in-hole insertion problems are analyzed. Firstly, all possible contact states are enumerated in three dimensions. Secondly, contact forces can be described by the screw theory. The screw theory gives a very compact and efficient formulation. Applying the static equilibrium equations, the conditions on applied forces and moments for maintaining each contact state are formulated. Thirdly, jamming diagrams are obtained. 33 kinds of possible jamming diagrams are analyzed. The force/moment conditions to guarantee successful insertion are obtained from all possible jamming diagrams. Then, some contact states are given, which finish a dual peg-in-hole process. Their geometric conditions are derived to verify the analyses.

2. Contact states classification of dual peg-in-hole

The geometric model of a dual peg-in-hole problem is shown in Fig. 1. Left peg has a radius of r_{P1}, whereas right peg has a radius of r_{P2}. The radii of left hole and right hole are r_{H1} and r_{H2}, respectively. D (D_P) represents the distance between the peg axes, and D_H represents the distance between the hole axes. The clearances between left peg and left hole, and between right peg and right hole are c_1 and c_2, respectively. To simplify our analysis, we only consider multiple pegs which are round, parallel and have the same length. Besides these, we make the following assumptions:

1) In the assembly process, the angle θ between the axes of the pegs and those of the holes is small and can be neglected.
2) Insertion direction is only vertically downward.
3) Quasi-static motion.
4) All pegs have the same length and are parallel.
5) All axes of the holes are parallel to each other, and perpendicular to the horizontal plane.
6) The clearances between pegs and holes are positive.

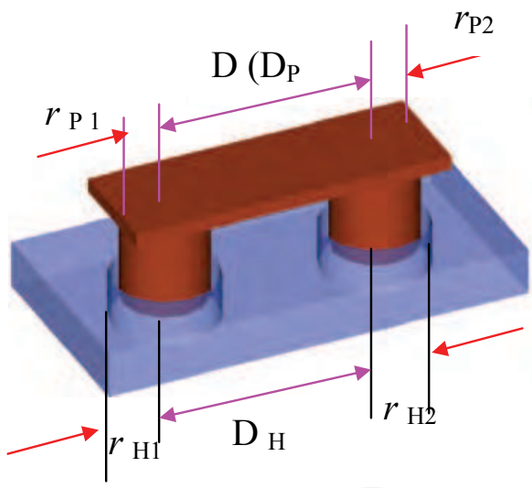

Fig. 1. Geometry of a dual peg-in-hole.

2.1 Contact states of a dual peg-in-hole in three dimensions

Because the uncertainty of geometry and control, contact states exist during the assembly process. For a dual peg-in-hole insertion, three-point contact states exist only when a certain set of conditions are satisfied. Three-point contact states or four-point contact states are transient and considered trivial (Sathirakul and Sturges, 1998). Thus, in the paper, one-point and two-point contact states will be analyzed in detail.

Expect three kinds of line contact states (Sathirakul and Sturges, 1998), there are ten kinds of point contact states when pegs tilt to the left, as shown in Table 1. Table 1 shows all possible point contact states of a dual peg-in-hole in three dimensions. The vectors of contact points, and the angular ranges between the vectors of contact forces and the x-axis can be seen in Table 1.

Dual peg-in-hole	Three dimensional contact states		α_i	r_i
When pegs tilt to the left, *k* stands for *l*. When pegs tilt to the right *k* stands for *r*.	One-point contact states	(*k*-1)	$\alpha_1 \in [0° \quad 90°] \cup [270° \quad 360°]$	$r_1 : (x_1 \quad y_1 \quad -jh_1)$
		(*k*-2)	$\alpha_2 \in [90° \quad 270°]$	$r_2 : (x_2 \quad y_2 \quad -(1-j)h_2)$
		(*k*-3)	$\alpha_3 \in [0° \quad 90°] \cup [270° \quad 360°]$	$r_3 : (x_3 \quad y_3 \quad -jh_3)$
		(*k*-4)	$\alpha_4 \in [90° \quad 270°]$	$r_4 : (x_4 \quad y_4 \quad -(1-j)h_4)$
	Two-point contact states	(*k*-5)	$\alpha_1 \in [0° \quad 90°] \cup [270° \quad 360°]$, $\alpha_2 \in [90° \quad 270°]$	$r_1 : (x_1 \quad y_1 \quad -jh_1)$, $r_2 : (x_2 \quad y_2 \quad -(1-j)h_2)$
		(*k*-6)	$\alpha_3 \in [0° \quad 90°] \cup [270° \quad 360°]$, $\alpha_4 \in [90° \quad 270°]$	$r_3 : (x_3 \quad y_3 \quad -jh_3)$, $r_4 : (x_4 \quad y_4 \quad -(1-j)h_4)$
		(*k*-7)	$\alpha_1 \in [0° \quad 90°] \cup [270° \quad 360°]$, $\alpha_3 \in [0° \quad 90°] \cup [270° \quad 360°]$	$r_1 : (x_1 \quad y_1 \quad -jh_1)$, $r_3 : (x_3 \quad y_3 \quad -jh_3)$
		(*k*-8)	$\alpha_1 \in [0° \quad 90°] \cup [270° \quad 360°]$, $\alpha_4 \in [90° \quad 270°]$	$r_1 : (x_1 \quad y_1 \quad -jh_1)$, $r_4 : (x_4 \quad y_4 \quad -(1-j)h_4)$
		(*k*-9)	$\alpha_2 \in [90° \quad 270°]$, $\alpha_3 \in [0° \quad 90°] \cup [270° \quad 360°]$	$r_2 : (x_2 \quad y_2 \quad -(1-j)h_2)$, $r_3 : (x_3 \quad y_3 \quad -jh_3)$
		(*k*-10)	$\alpha_2 \in [90° \quad 270°]$, $\alpha_4 \in [90° \quad 270°]$	$r_2 : (x_2 \quad y_2 \quad -(1-j)h_2)$, $r_4 : (x_4 \quad y_4 \quad -(1-j)h_4)$
When pegs tilt to the left *j*=1. When pegs tilt to the right *j*=0.				

Table 1. Assembly contact states of a dual peg-in-hole in three dimensions.

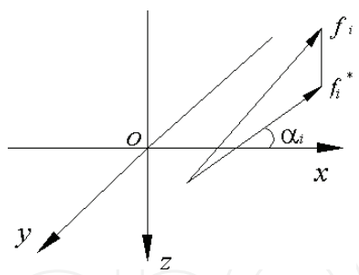

Fig. 2. α_i between the vector f_i * and the x-axis.

The coordinate system oxyz is set up at the center of dual pegs. Here *i*=1 represents that the left peg and left hole contact in the left, *i*=2 represents that the left peg and left hole contact in the right, *i*=3 represents that the right peg and right hole contact in the left, *i*=4 represents that the right peg and right hole contact in the right. *i*=1 or *i*=3 represents left-contact; *i*=2 or *i*=4 represents right-contact. Left-contact is the situation in which the left or right peg makes contacts with its hole in the left; Right-contact is the situation in which the left or right peg makes contacts with its hole in the right. Mapping the contact force f_i to the plane xoy, the corresponding vector f_i * can be obtained; α_i is an angle between the vector f_i * and the x-axis (Fig. 2). According to the above assumption, θ is small and can be neglected. Thus, f_i * is equal to f_i ; r_i is a vector which represents contact point's position in fixed coordinate system oxyz; h_i is an insertion depth; μ is friction coefficient. According to the above analysis, there are also ten kinds of contact states when pegs tilt to the right (Table 1).

For example, let pegs tilt to the left, if i=1, one-point contact state (l-1) exists. If i=1and i=4, two-point contact state (l-8) exists (Fig. 3). Let pegs tilt to the right, If i=1, one-point contact state (r-4) exists; if i=1and i=4, two-point contact state (r-8) exists (Fig. 3). During the insertion, the dual-peg may undergo several contact states. In the paper, some states can be chosen, such as, pegs tilting to the left: state (l-1), state (l-5), state (l-8), a possible three-point contact state and a mating state or pegs tilting to the right: state (r-4), state (r-6), state (r-8), a possible three-point contact state and a mating state to finish a dual peg-in-hole assembly process. Their three dimensional charts and two dimensional charts are shown in Fig. 3 and Fig. 4.

2.2 Contact states of a dual peg-in-hole in two dimensions

When α_i=0° or 180°, three dimensional problems can be simplified to two dimensional problems. The two dimensional chart of each state in Fig. 3 is shown in Fig. 4.

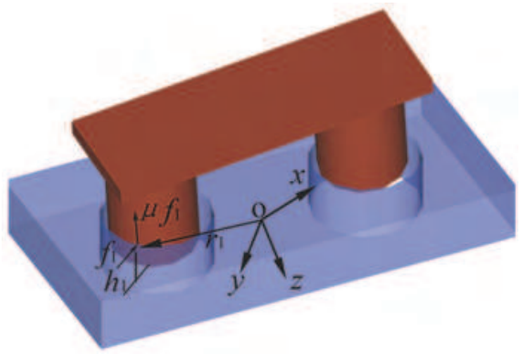

(state l-1): $\alpha_1 \in [0° \quad 90°] \cup [270° \quad 360°]$, $r_1 : (x_1 \quad y_1 \quad -h_1)$

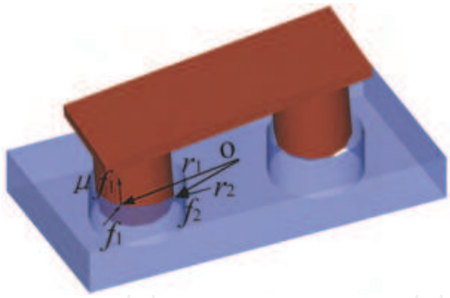

$\alpha_1 \in [0° \quad 90°] \cup [270° \quad 360°]$, $\alpha_2 \in [90° \quad 270°]$

$r_1 : (x_1 \quad y_1 \quad -h_1)$, $r_2 : (x_2 \quad y_2 \quad 0)$

(state l-5)

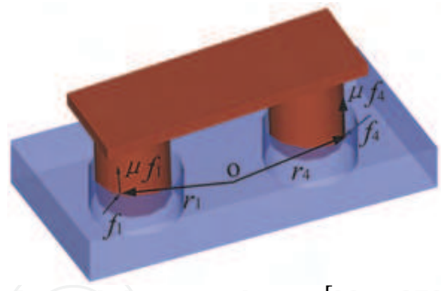

$\alpha_1 \in [0° \quad 90°] \cup [270° \quad 360°]$, $\alpha_4 \in [90° \quad 270°]$

$r_1 : (x_1 \quad y_1 \quad -h_1)$, $r_4 : (x_4 \quad y_4 \quad 0)$

(state l-8)

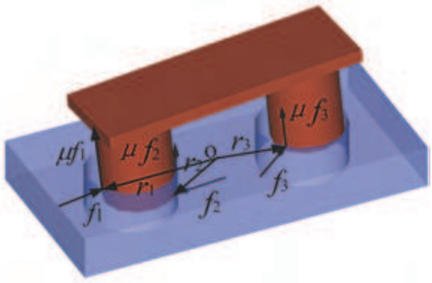

a possible three-point contact state

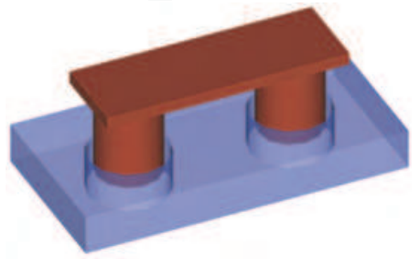

mating state

(a) pegs tilt to the left

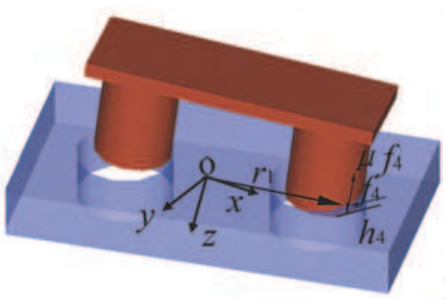

(state *r*-4)

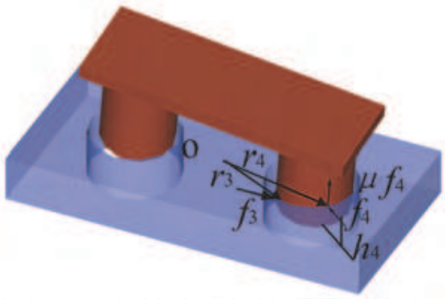

(state *r*-6)

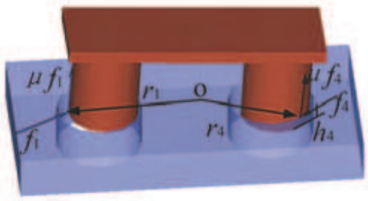

(state *r*-8)

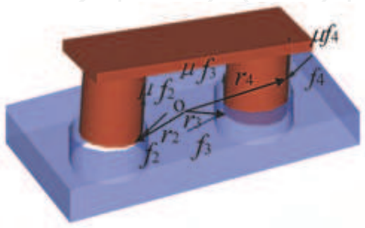

a possible three-point contact state

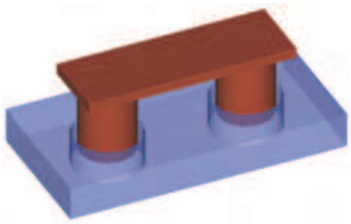

mating state

(b) pegs tilt to the right

Fig. 3. Assembly states of a dual peg-in-hole in three dimensions.

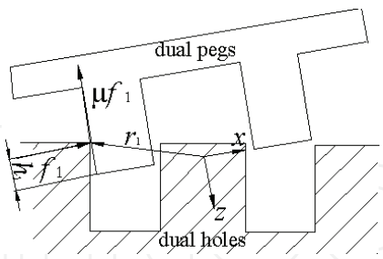

(state *l*-1) (α_1=0°)

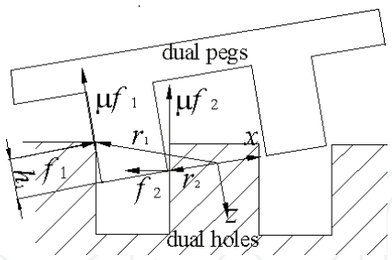

(state *l*-5) (α_1=0°, α_2=180°)

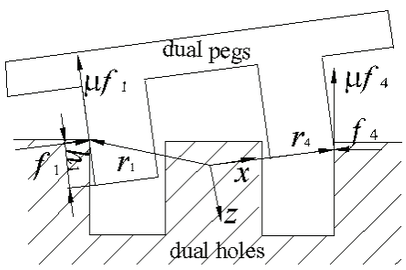

(state *l*-8) (α_1=0°, α_4=180°)

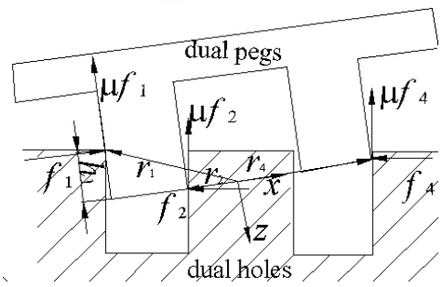

a possible three-point contact state

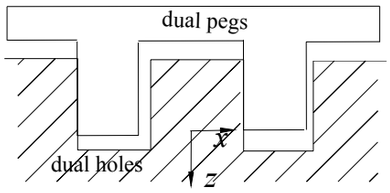

mating state

(a) pegs tilt to the left

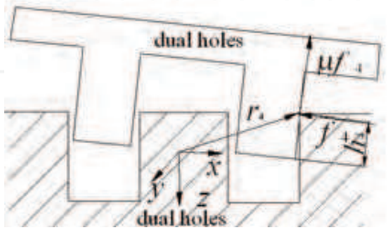

state *r*-4 (α_{4}=180°)

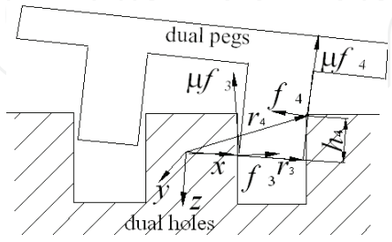

state *r*-6 (α_{3}=0°, α_{4}=180°)

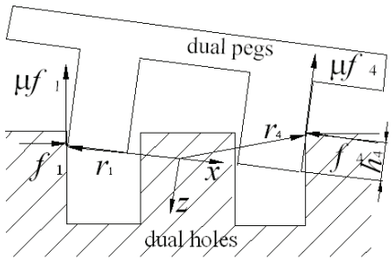

state *r*-8(α_{1}=0°, α_{4}=180°)

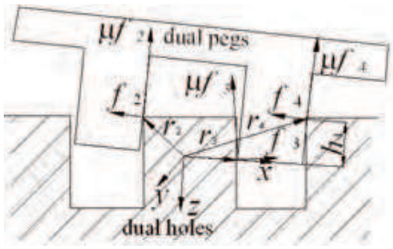

a possible three-point contact state

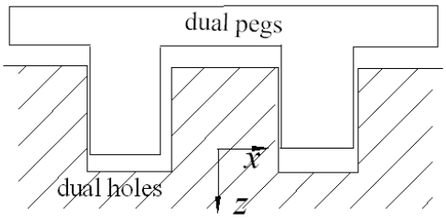

mating state

(b) pegs tilt to the right

Fig. 4. Assembly states of a dual peg-in-hole in two dimensions.

3. Geometric constraints and contact states analysis

According to the above chosen states (pegs tilting to the left: state *l*-1, state *l*-5, state *l*-8, a possible three-point contact state and a mating state or pegs tilting to the right: state *r*-4, state *r*-6, state *r*-8, a possible three-point contact state and a mating state), the relations between these states and their geometric constraints are analyzed. Thus, the complexity of the three dimensional dual peg-in-hole can be known. The dimensions of a dual peg and a dual hole are given as follows (Fig. 1): $2r_{P_1} = 2r_{P_2} = 9.9mm$, $2r_{H_1} = 2r_{H_2} = 10.0mm$, $D_P = 90.2mm$, $D_H = 90.25mm$, $C_1 = C_2 = 0.075mm$, μ=0.1.

3.1 Two dimensions

The boundary state of state *l*-1 or state *r*-4 is shown in Fig. 5. Its geometric constraint is

$$\begin{cases} h_0 s\theta_0 + 2r_{P_1} c\theta_0 = 2r_{H_1} \\ h_0 c\theta_0 = 2r_{P_1} s\theta_0 \end{cases} \tag{1}$$

Thus,θ_0=8.1°, h_0=1.397mm can be obtained. When θ is less than θ_0, state *l*-1 or state *r*-4 can be reached.

According to Fig. 3, for pegs tilting to the left, the geometric constraint of state *l*-5 can be expressed as,

$$h_1 s\theta + 2r_{P_1} c\theta = 2r_{H_1} \tag{2a}$$

The geometric constraint of state *l*-8 can be expressed as,

$$h_1 s\theta + \left(D_P + r_{P_2} + r_{P_1}\right) c\theta = \left(D_H + r_{H_2} + r_{H_1}\right) \tag{3a}$$

According to Fig. 3, for pegs tilting to the right, the geometric constraint condition of state *r*-6 in two dimensions can be expressed as,

$$h_4 s\theta + 2r_{P_1} c\theta = 2r_{H_1} \tag{2b}$$

The geometric constraint condition of state *r*-8 in two dimensions can be expressed as,

$$h_4 s\theta + \left(D_P + r_{P_2} + r_{P_1}\right) c\theta = \left(D_H + r_{H_2} + r_{H_1}\right) \tag{3b}$$

If Eqs. (2a) and (3a) or Eqs. (2b) and (3b) have one solution at least, a three-point contact state of two dimensional dual peg-in-hole can be reached. Fig.6 suggests that a three-point contact state is relative to the geometry of assembly objects. At the point where two curves of plots intersect, the three-point contact states can exist. From Fig. 6, we can see that three-point contact states are transient. Hereθ_0 andθ are angles between the axes of a peg and a hole, h_0 and h_i are insertion depths.

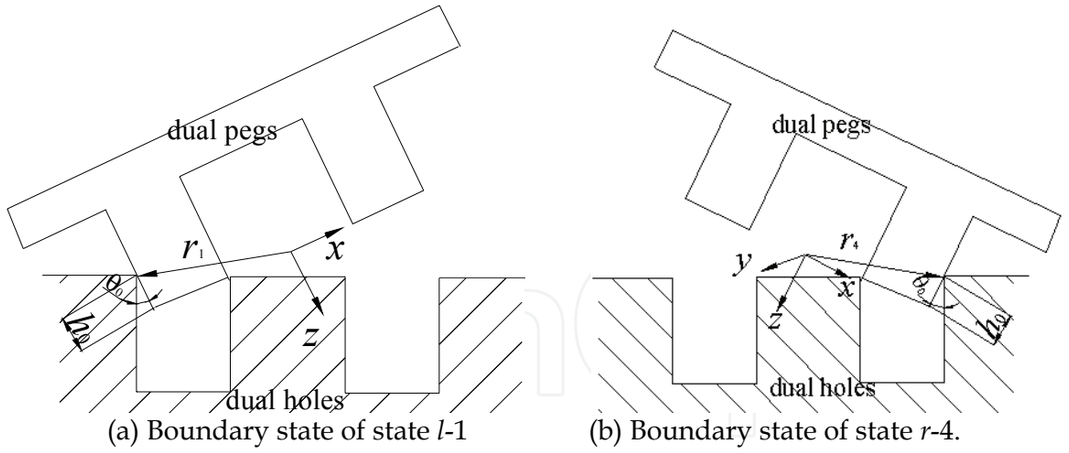

(a) Boundary state of state *l*-1 (b) Boundary state of state *r*-4.

Fig. 5. Boundary state.

3.2 Three dimensions

Three dimensional multiple peg-in-hole problems are more complex than two dimensional peg-in-hole problems. But they have similar geometric constraint conditions. For the boundary state of state *l*-1 or state *r*-4 in three dimensions, we can obtain:

$$\begin{cases} h_0 s\theta_0 + 2r'_{P_1} c\theta_0 = 2r'_{H_1} \\ h_0 c\theta_0 = 2r'_{P_1} s\theta_0 \end{cases}, \; r'_{P_1} \le r_{P_1}, \; r'_{H_1} \le r_{H_1} \tag{4}$$

If $\theta < \theta_0$, state *l*-1 or state *r*-4 can be reached.

For state *l*-5 in three dimensions, we can obtain the following formulas:

$$h_1 s\theta + 2r'_{P_1} c\theta = 2r'_{H_1},\ r'_{P_1} \le r_{P_1},\ r'_{H_1} \le r_{H_1} \tag{5a}$$

For state *l*-8 in three dimensions, we can obtain the following formulas:

$$h_1 s\theta + \left(D'_P + r'_{P_2} + r'_{P_1}\right) c\theta = \left(D'_H + r'_{H_2} + r'_{H_1}\right),$$

$$r'_{P_1} \le r_{P_1},\ r'_{P_2} \le r_{P_2},\ D'_P \le D_P,\ r'_{H_1} \le r_{H_1},\ r'_{H_2} \le r_{H_2},\ D'_H \le D_H \tag{6a}$$

For state *r*-6 in three dimensions, we can obtain the following constraint formulas:

$$h_4 s\theta + 2r'_{P_1} c\theta = 2r'_{H_1},\ r'_{P_1} \le r_{P_1},\ r'_{H_1} \le r_{H_1} \tag{5b}$$

For state *r*-8 in three dimensions, we can obtain the following formulas:

$$h_4 s\theta + \left(D'_P + r'_{P_2} + r'_{P_1}\right) c\theta = \left(D'_H + r'_{H_2} + r'_{H_1}\right),$$

$$r'_{P_1} \le r_{P_1},\ r'_{P_2} \le r_{P_2},\ D'_P \le D_P,\ r'_{H_1} \le r_{H_1},\ r'_{H_2} \le r_{H_2},\ D'_H \le D_H \tag{6b}$$

If constraint conditions are formulas (5a) and (6a) or (5b) and (6b) at the same time, three-point contact states of the three dimensional peg-in-hole can be obtained.

Mapping two contact points on the peg to the plane xoy, we can obtain two corresponding points. The distance between these two points is $2r'_{P_1}$ ($2r'_{P_2}$). $2r'_{H_1}$ or $2r'_{H_2}$ represents the distance between two contact points on the left hole or on the right hole, respectively. Mapping one contact point on the left peg and the other contact point on the right peg to the plane xoy, we can obtain two corresponding points. The distance between these two points is D'_P. D'_H represents the distance between one contact points on the left hole and the other contact point on the right hole.

According to the analysis of the two dimensional dual peg-in-hole, the following results can be inferred in three dimensions. For different contact geometric dimensions (such as r'_{P_1}, r'_{P_2}, D'_P, r'_{H_1}, r'_{H_2} and D'_H) of the three dimensional dual peg-in-hole, state *l*-5 and state *l*-8 show different curves, but their change trends are similar. At the point where two curves of state *l*-5 and state *l*-8 intersect, three-point contact states can exist, which are relative to the geometry of assembly objects. It means that three-point contact states, in 3D cases, can exist only when a certain set of conditions are satisfied. They are transient and considered trivial.

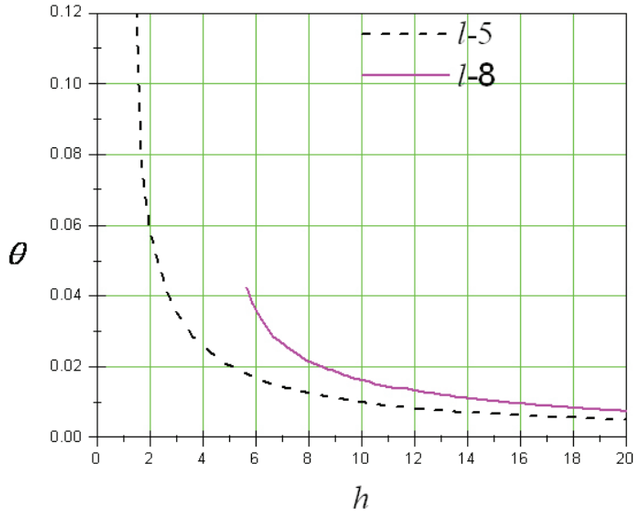

Fig. 6. θ vs *h* of state *l*-5 and state *l*-8 in two dimensions.

4. Analyzing contact force/moment of three dimensional dual peg-in-hole based on the screw theory

By understanding the physics of assembly processes, one can plan fine motion strategies and guarantee successful operations. An analysis of forces and moments during the three dimensional dual-peg insertion is important in planning fine motions. In order to insert dual pegs into their holes, insertion forces and moments $\begin{pmatrix} F_x & F_y & F_z & M_x & M_y & M_z \end{pmatrix}$ applied to the pegs at point *o* have to satisfy a number of conditions. In this section, the conditions on applied forces and moments for maintaining each contact state are derived. Then jamming conditions are obtained. These are basic conditions of fine motions and can avoid unsuccessful insertions. The conditions which guarantee successful insertions can be obtained from the jamming diagrams.

As mentioned previously, there are 20 kinds of point contact states expect 6 kinds of line contact states. The contact states that have more than 2 contacts are ignored. According to a series of chosen contact states in Fig. 3, forces and moments can be described by screw theory (Tsaprounis, 1998). Because a quasi-static process is assumed, each of the contact states is analyzed from static equilibrium conditions. With the static equilibrium conditions and geometric constraints, the relationship between moments and forces is analyzed. The coordinate system (oxyz) is set up at the center of dual pegs and contact forces are shown in Fig. 3,4. The dual-peg is about to move down or is moving down. Examples of one-point contact state *l*-1 or state *r*-4 and two-point contact state *l*-8 or state *r*-8 are analyzed in detail. The relationship between forces and moments of other contact states can be analyzed similarly (Table 2). Table 2 shows the relationship between forces and moments of all possible point contact states about the three dimensional dual peg-in-hole.

The wrenches of the contact cases are described as follows

$$\hat{\mathbf{F}}_i = \mathbf{F}_i + \varepsilon(\mathbf{F}_i \times \mathbf{r}_i) \tag{7}$$

$$\hat{\mathbf{f}}_i = \mathbf{f}_i + \varepsilon(\mathbf{f}_i \times \mathbf{r}_i) \tag{8}$$

$$f_i = \mu F_i$$

$\hat{\mathbf{F}}_i$ is the wrench of the contact force; $\hat{\mathbf{f}}_i$ is the wrench of the friction force corresponding to the contact force. The real parts of the above equations (7) and (8) express the contact forces and the dual parts express the moments. Thus, we can obtain

$$\hat{\mathbf{F}}_i : \begin{pmatrix} \mathbf{F}_{ix} & \mathbf{F}_{iy} & \mathbf{F}_{iz} & (\mathbf{F}_i \times \mathbf{r}_i)_x & (\mathbf{F}_i \times \mathbf{r}_i)_y & (\mathbf{F}_i \times \mathbf{r}_i)_z \end{pmatrix}$$

$$\hat{\mathbf{f}}_i : \begin{pmatrix} \mathbf{f}_{ix} & \mathbf{f}_{iy} & \mathbf{f}_{iz} & (\mathbf{f}_i \times \mathbf{r}_i)_x & (\mathbf{f}_i \times \mathbf{r}_i)_y & (\mathbf{f}_i \times \mathbf{r}_i)_z \end{pmatrix}$$

(1) One-point contact state *l*-1 and state *r*-4:

State *l*-1: the compact forms of the wrenches of contact forces in contact points are described as follows,

$$\begin{pmatrix} f_1 c\alpha_1 & f_1 s\alpha_1 & 0 & h_1 f_1 s\alpha_1 & -h_1 f_1 c\alpha_1 & x_1 f_1 s\alpha_1 - y_1 f_1 c\alpha_1 \end{pmatrix}$$

$$\begin{pmatrix} 0 & 0 & -\mu f_1 & -y_1 \mu f_1 & x_1 \mu f_1 & 0 \end{pmatrix}$$

The wrenches of the assembly forces are described as follows $\begin{pmatrix} F_x & F_y & F_z & M_x & M_y & M_z \end{pmatrix}$.

According to the static equilibrium equations, we can obtain

$$\begin{cases} \mathrm{F_x} + f_1 c\alpha_1 = 0 \\ F_y + f_1 s\alpha_1 = 0 \\ F_z - \mu f_1 = 0 \\ M_x + h_1 f_1 s\alpha_1 - y_1 \mu f_1 = 0 \\ M_y - h_1 f_1 c\alpha_1 + x_1 \mu f_1 = 0 \\ M_z + x_1 f_1 s\alpha_1 - y_1 f_1 c\alpha_1 = 0 \end{cases} \tag{9}$$

From Eq. (9), we can obtain the following relationship equations,

$$\begin{cases} \dfrac{F_x}{F_z} = -\dfrac{c\alpha_1}{\mu} \\ \dfrac{M_y}{F_z} = \dfrac{h_1 c\alpha_1}{\mu} - x_1 \end{cases} \tag{10}$$

$$\begin{cases} \dfrac{F_y}{F_z} = -\dfrac{s\alpha_1}{\mu} \\ \dfrac{M_x}{F_z} = -\dfrac{h_1 s\alpha_1}{\mu} + y_1 \end{cases} \tag{11}$$

where $\alpha_1 \in [0° \quad 90°] \cup [270° \quad 360°]$, $r_1 : (x_1 \quad y_1 \quad -h_1)$.

State *r*-4: the wrenches of contact forces in contact points are as follows,

$$\begin{matrix} (f_4 c\alpha_4 & f_4 s\alpha_4 & 0 & h_4 f_4 s\alpha_4 & -h_4 f_4 c\alpha_4 & x_4 f_4 s\alpha_4 - y_4 f_4 c\alpha_4) \\ (0 & 0 & -\mu f_4 & -y_4 \mu f_4 & x_4 \mu f_4 & 0) \end{matrix}$$

The wrenches of the assembly forces are as follows $(F_x \quad F_y \quad F_z \quad M_x \quad M_y \quad M_z)$.

According to the static equilibrium equations, we can obtain

$$\begin{cases} \mathrm{F_x} + f_4 c\alpha_4 = 0 \\ F_y + f_4 s\alpha_4 = 0 \\ F_z - \mu f_4 = 0 \\ M_x + h_4 f_4 s\alpha_4 - y_4 \mu f_4 = 0 \\ M_y - h_4 f_4 c\alpha_4 + x_4 \mu f_4 = 0 \\ M_z + x_4 f_4 s\alpha_4 - y_4 f_4 c\alpha_4 = 0 \end{cases} \tag{12}$$

Thus, we can obtain the following relationship equations,

$$\begin{cases} \dfrac{F_x}{F_z} = -\dfrac{c\alpha_4}{\mu} \\ \dfrac{M_y}{F_z} = \dfrac{h_4 c\alpha_4}{\mu} - x_4 \end{cases} \tag{13}$$

$$\begin{cases} \dfrac{F_y}{F_z} = -\dfrac{s\alpha_4}{\mu} \\ \dfrac{M_x}{F_z} = -\dfrac{h_4 s\alpha_4}{\mu} + y_4 \end{cases} \tag{14}$$

where $\alpha_4 \in [90° \quad 270°]$, $r_4 : (x_4 \quad y_4 \quad -h_4)$.

(2) two-point contact state *l*-8 and state *r*-8:

State *l*-8: the compact forms of the wrenches of contact forces in contact points are described as follows,

$$\begin{pmatrix} f_1c\alpha_1 & f_1s\alpha_1 & 0 & h_1f_1s\alpha_1 & -h_1f_1c\alpha_1 & x_1f_1s\alpha_1 - y_1f_1c\alpha_1 \end{pmatrix}$$
$$\begin{pmatrix} 0 & 0 & -\mu f_1 & -y_1\mu f_1 & x_1\mu f_1 & 0 \end{pmatrix}$$
$$\begin{pmatrix} f_4c\alpha_4 & f_4s\alpha_4 & 0 & 0 & 0 & x_4f_4s\alpha_4 - y_4f_4c\alpha_4 \end{pmatrix}$$
$$\begin{pmatrix} 0 & 0 & -\mu f_4 & -y_4\mu f_4 & x_4\mu f_4 & 0 \end{pmatrix}$$

The wrenches of the assembly forces are as follows, $\begin{pmatrix} F_x & F_y & F_z & M_x & M_y & M_z \end{pmatrix}$.

According to the static equilibrium equations, we obtain the expressions of moments M_y, M_x in terms of insertion forces as:

$$\frac{M_y}{DF_z} = -\frac{\mu}{c\alpha_1 - c\alpha_4}\left[\frac{x_4 - x_1}{D} + \frac{h_1c\alpha_1}{\mu D}\right]\frac{F_x}{F_z} + \frac{\mu x_1c\alpha_4 - \mu x_4c\alpha_1 - h_1c\alpha_1c\alpha_4}{\mu D(c\alpha_1 - c\alpha_4)} \tag{15}$$

$$\frac{M_x}{DF_z} = -\frac{\mu}{s\alpha_1 - s\alpha_4}\left[-\frac{y_4 - y_1}{D} - \frac{h_1s\alpha_1}{\mu D}\right]\frac{F_y}{F_z} + \frac{-\mu y_1s\alpha_4 + \mu y_4s\alpha_1 + h_1s\alpha_1s\alpha_4}{\mu D(s\alpha_1 - s\alpha_4)} \tag{16}$$

Eqs. (15) and (16) show linear relations, respectively. For Eq. (15), when $\frac{F_x}{F_z} = -\frac{c\alpha_1}{\mu}$, this equation reduces to Eq.(10). We can write $\frac{M_y}{DF_z} = \frac{h_1c\alpha_1}{\mu D} - \frac{x_1}{D}$. When $\frac{F_x}{F_z} = -\frac{c\alpha_4}{\mu}$, we can write $\frac{M_y}{DF_z} = -\frac{x_4}{D}$ (in Fig. 7(a)). For Eq. (16), when $\frac{F_y}{F_z} = -\frac{s\alpha_1}{\mu}$, this equation reduces to Eq.(11). We can write $\frac{M_x}{DF_z} = -\frac{h_1s\alpha_1}{\mu D} + \frac{y_1}{D}$. When $\frac{F_y}{F_z} = -\frac{s\alpha_2}{\mu}$, we can write $\frac{M_x}{DF_z} = \frac{y_4}{D}$ (in Fig. 7(b), Fig. 7(c)).

where $\alpha_1 \in [0° \quad 90°] \cup [270° \quad 360°]$, $\alpha_4 \in [90° \quad 270°]$, $r_1 : (x_1 \quad y_1 \quad -h_1)$, $r_4 : (x_4 \quad y_4 \quad 0)$.

State *r*-8: the wrenches of contact forces in contact points are as follows,

$$\begin{pmatrix} f_1c\alpha_1 & f_1s\alpha_1 & 0 & 0 & 0 & x_1f_1s\alpha_1 - y_1f_1c\alpha_1 \end{pmatrix}$$
$$\begin{pmatrix} 0 & 0 & -\mu f_1 & -y_1\mu f_1 & x_1\mu f_1 & 0 \end{pmatrix}$$
$$\begin{pmatrix} f_4c\alpha_4 & f_4s\alpha_4 & 0 & h_4f_4s\alpha_4 & -h_4f_4c\alpha_4 & x_4f_4s\alpha_4 - y_4f_4c\alpha_4 \end{pmatrix}$$
$$\begin{pmatrix} 0 & 0 & -\mu f_4 & -y_4\mu f_4 & x_4\mu f_4 & 0 \end{pmatrix}$$

The wrenches of the assembly forces are as follows, $\begin{pmatrix} F_x & F_y & F_z & M_x & M_y & M_z \end{pmatrix}$.

According to the static equilibrium equations, the following equations can be obtained,

$$\frac{M_y}{DF_z} = -\frac{\mu}{c\alpha_4 - c\alpha_1}\left[\frac{x_1 - x_4}{D} + \frac{h_4c\alpha_4}{\mu D}\right]\frac{F_x}{F_z} + \frac{\mu x_4c\alpha_1 - \mu x_1c\alpha_4 - h_4c\alpha_1c\alpha_4}{\mu D(c\alpha_4 - c\alpha_1)} \tag{17}$$

$$\frac{M_x}{DF_z} = -\frac{\mu}{s\alpha_4 - s\alpha_1}\left[-\frac{y_1 - y_4}{D} - \frac{h_4s\alpha_4}{\mu D}\right]\frac{F_y}{F_z} + \frac{-\mu y_4s\alpha_1 + \mu y_1s\alpha_4 + h_4s\alpha_1s\alpha_4}{\mu D(s\alpha_4 - s\alpha_1)} \tag{18}$$

Eqs. (17) and (18) show linear relations. For Eq. (17), when $\frac{F_x}{F_z} = -\frac{c\alpha_1}{\mu}$, we can write $\frac{M_y}{DF_z} = -\frac{x_1}{D}$. When $\frac{F_x}{F_z} = -\frac{c\alpha_4}{\mu}$, we can write $\frac{M_y}{DF_z} = \frac{h_4c\alpha_4}{\mu D} - \frac{x_4}{D}$. For Eq. (18), when

$\frac{F_y}{F_z}=-\frac{s\alpha_1}{\mu}$, we can write $\frac{M_x}{DF_z}=\frac{y_1}{D}$. When $\frac{F_y}{F_z}=-\frac{s\alpha_4}{\mu}$, we can write $\frac{M_x}{DF_z}=-\frac{h_4 s\alpha_4}{\mu D}+\frac{y_4}{D}$.

where $\alpha_1\in[0^\circ \quad 90^\circ]\cup[270^\circ \quad 360^\circ]$, $\alpha_4\in[90^\circ \quad 270^\circ]$, $r_1:(x_1 \quad y_1 \quad 0)$, $r_4:(x_4 \quad y_4 \quad -h_4)$.

(3) The compact forms of the wrenches of three-point contact can be described as follows,

$$(f_1c\alpha_1 \quad f_1s\alpha_1 \quad 0 \quad h_1f_1s\alpha_1 \quad -h_1f_1c\alpha_1 \quad x_1f_1s\alpha_1-y_1f_1c\alpha_1)$$
$$(0 \quad 0 \quad -\mu f_1 \quad -y_1\mu f_1 \quad x_1\mu f_1 \quad 0)$$
$$(f_2c\alpha_2 \quad f_2s\alpha_2 \quad 0 \quad 0 \quad 0 \quad x_2f_2s\alpha_2-y_2f_2c\alpha_2)$$
$$(0 \quad 0 \quad -\mu f_2 \quad -y_2\mu f_2 \quad x_2\mu f_2 \quad 0)$$
$$(f_3c\alpha_3 \quad f_3s\alpha_3 \quad 0 \quad h_3f_3s\alpha_3 \quad -h_3f_3c\alpha_3 \quad x_3f_3s\alpha_3-y_3f_3c\alpha_3)$$
$$(0 \quad 0 \quad -\mu f_3 \quad -y_3\mu f_3 \quad x_3\mu f_3 \quad 0)$$

Because three-point contact states are transient and considered trivial, their analysis is ignored.

Three dimensional contact states		Force/moment of contact states
One-point contact states	(k-1)	$\begin{cases}\frac{F_x}{F_z}=-\frac{c\alpha_1}{\mu}\\ \frac{M_y}{F_z}=j\frac{h_1c\alpha_1}{\mu}-x_1\end{cases}$ $\begin{cases}\frac{F_y}{F_z}=-\frac{s\alpha_1}{\mu}\\ \frac{M_x}{F_z}=-j\frac{h_1s\alpha_1}{\mu}+y_1\end{cases}$
	(k-2)	$\begin{cases}\frac{F_x}{F_z}=-\frac{c\alpha_2}{\mu}\\ \frac{M_y}{F_z}=(1-j)\frac{h_2c\alpha_2}{\mu}-x_2\end{cases}$ $\begin{cases}\frac{F_y}{F_z}=-\frac{s\alpha_2}{\mu}\\ \frac{M_x}{F_z}=-(1-j)\frac{h_2s\alpha_2}{\mu}+y_2\end{cases}$
	(k-3)	$\begin{cases}\frac{F_x}{F_z}=-\frac{c\alpha_3}{\mu}\\ \frac{M_y}{F_z}=j\frac{h_3c\alpha_3}{\mu}-x_3\end{cases}$ $\begin{cases}\frac{F_y}{F_z}=-\frac{s\alpha_3}{\mu}\\ \frac{M_x}{F_z}=-j\frac{h_3s\alpha_3}{\mu}+y_3\end{cases}$
	(k-4)	$\begin{cases}\frac{F_x}{F_z}=-\frac{c\alpha_4}{\mu}\\ \frac{M_y}{F_z}=(1-j)\frac{h_4c\alpha_4}{\mu}-x_4\end{cases}$ $\begin{cases}\frac{F_y}{F_z}=-\frac{s\alpha_4}{\mu}\\ \frac{M_x}{F_z}=-(1-j)\frac{h_4s\alpha_4}{\mu}+y_4\end{cases}$
	(k-5)	$\frac{M_y}{DF_z}=-\frac{\mu}{c\alpha_1-c\alpha_2}\left[\frac{x_2-x_1}{D}+j\frac{h_1c\alpha_1}{\mu D}-(1-j)\frac{h_2c\alpha_2}{\mu D}\right]\frac{F_x}{F_z}+\frac{\mu x_1c\alpha_2-\mu x_2c\alpha_1-jh_1c\alpha_1c\alpha_2+(1-j)h_2c\alpha_1c\alpha_2}{\mu D(c\alpha_1-c\alpha_2)}$ $\frac{M_x}{DF_z}=-\frac{\mu}{s\alpha_1-s\alpha_2}\left[-\frac{y_2-y_1}{D}-j\frac{h_1s\alpha_1}{\mu D}+(1-j)\frac{h_2s\alpha_2}{\mu D}\right]\frac{F_y}{F_z}+\frac{-\mu y_1s\alpha_2+\mu y_2s\alpha_1+jh_1s\alpha_1s\alpha_2-(1-j)h_2s\alpha_1s\alpha_2}{\mu D(s\alpha_1-s\alpha_2)}$
	(k-6)	$\frac{M_y}{DF_z}=-\frac{\mu}{c\alpha_3-c\alpha_4}\left[\frac{x_4-x_3}{D}+j\frac{h_3c\alpha_3}{\mu D}-(1-j)\frac{h_4c\alpha_4}{\mu D}\right]\frac{F_x}{F_z}+\frac{\mu x_3c\alpha_4-\mu x_4c\alpha_3-jh_3c\alpha_3c\alpha_4+(1-j)h_4c\alpha_3c\alpha_4}{\mu D(c\alpha_3-c\alpha_4)}$ $\frac{M_x}{DF_z}=-\frac{\mu}{s\alpha_3-s\alpha_4}\left[-\frac{y_4-y_3}{D}-j\frac{h_3s\alpha_3}{\mu D}+(1-j)\frac{h_4s\alpha_4}{\mu D}\right]\frac{F_y}{F_z}+\frac{-\mu y_3s\alpha_4+\mu y_4s\alpha_3+jh_3s\alpha_3s\alpha_4-(1-j)h_4s\alpha_3s\alpha_4}{\mu D(s\alpha_3-s\alpha_4)}$

two-point contact states	(*k*-7)	$\frac{M_y}{DF_z}=\frac{\mu}{c\alpha_1-c\alpha_3}\left(\frac{x_1-x_3}{D}+j\frac{-h_1c\alpha_1+h_3c\alpha_3}{\mu D}\right)\frac{F_x}{F_z}+\frac{x_1\mu c\alpha_3-x_3\mu c\alpha_1+j(-h_1c\alpha_1c\alpha_3+h_3c\alpha_1c\alpha_3)}{\mu D(c\alpha_1-c\alpha_3)}$ $\frac{M_x}{DF_z}=-\frac{\mu}{s\alpha_1-s\alpha_3}\left(\frac{y_1-y_3}{D}+j\frac{-h_1s\alpha_1+h_3s\alpha_3}{\mu D}\right)\frac{F_y}{F_z}+\frac{y_3\mu s\alpha_1-y_1\mu s\alpha_3+j(h_1s\alpha_1s\alpha_3-h_3s\alpha_1s\alpha_3)}{\mu D(s\alpha_1-s\alpha_3)}$
	(*k*-8)	$\frac{M_y}{DF_z}=-\frac{\mu}{c\alpha_1-c\alpha_4}\left[\frac{x_4-x_1}{D}+j\frac{h_1c\alpha_1}{\mu D}-(1-j)\frac{h_4c\alpha_4}{\mu D}\right]\frac{F_x}{F_z}+\frac{\mu x_1c\alpha_4-\mu x_4c\alpha_1-jh_1c\alpha_1c\alpha_4+(1-j)h_4c\alpha_1c\alpha_4}{\mu D(c\alpha_1-c\alpha_4)}$ $\frac{M_x}{DF_z}=-\frac{\mu}{s\alpha_1-s\alpha_4}\left[-\frac{y_4-y_1}{D}-j\frac{h_1s\alpha_1}{\mu D}+(1-j)\frac{h_4s\alpha_4}{\mu D}\right]\frac{F_y}{F_z}+\frac{-\mu y_1s\alpha_4+\mu y_4s\alpha_1+jh_1s\alpha_1s\alpha_4-(1-j)h_4s\alpha_1s\alpha_4}{\mu D(s\alpha_1-s\alpha_4)}$
	(*k*-9)	$\frac{M_y}{DF_z}=-\frac{\mu}{c\alpha_3-c\alpha_2}\left[\frac{x_2-x_3}{D}+j\frac{h_3c\alpha_3}{\mu D}-(1-j)\frac{h_2c\alpha_2}{\mu D}\right]\frac{F_x}{F_z}+\frac{\mu x_3c\alpha_2-\mu x_2c\alpha_3-jh_3c\alpha_3c\alpha_2+(1-j)h_2c\alpha_2c\alpha_3}{\mu D(c\alpha_3-c\alpha_2)}$ $\frac{M_x}{DF_z}=-\frac{\mu}{s\alpha_3-s\alpha_2}\left[-\frac{y_2-y_3}{D}-j\frac{h_3s\alpha_3}{\mu D}+(1-j)\frac{h_2s\alpha_2}{\mu D}\right]\frac{F_y}{F_z}+\frac{-\mu y_3s\alpha_2+\mu y_2s\alpha_3+jh_3s\alpha_3s\alpha_2-(1-j)h_2s\alpha_2s\alpha_3}{\mu D(s\alpha_3-s\alpha_2)}$
	(*k*-10)	$\frac{M_y}{DF_z}=\frac{\mu}{c\alpha_2-c\alpha_4}\left(\frac{x_2-x_4}{D}+(1-j)\frac{-h_2c\alpha_2+h_4c\alpha_4}{\mu D}\right)\frac{F_x}{F_z}+\frac{\mu x_2c\alpha_4-\mu x_4c\alpha_2+(1-j)(-h_2c\alpha_2c\alpha_4+h_4c\alpha_2c\alpha_4)}{\mu D(c\alpha_2-c\alpha_4)}$ $\frac{M_x}{DF_z}=-\frac{\mu}{s\alpha_2-s\alpha_4}\left(\frac{y_2-y_4}{D}+(1-j)\frac{-h_2s\alpha_2+h_4s\alpha_4}{\mu D}\right)\frac{F_y}{F_z}+\frac{\mu y_4s\alpha_2-\mu y_2s\alpha_4+(1-j)(h_2s\alpha_2s\alpha_4-h_4s\alpha_2s\alpha_4)}{\mu D(s\alpha_2-s\alpha_4)}$
When pegs tilt to the left, *k* stands for *l* and *j*=1. When pegs tilt to the right, *k* stands for *r* and *j*=0.		

Table 2. Force/moment of contact states about the three dimensional dual peg-in-hole.

5. Jamming diagrams of three dimensional dual peg-in-hole

Jamming is a condition in which the peg will not move because the forces and moments applied to the peg through the support are in the wrong proportions (Whitney, 1982).

5.1 Jamming diagrams

Because the relation between forces and moments is not proper, pegs are struck in the holes and jamming appears. In this section, according the relations between $\frac{M_y}{F_z}$ and $\frac{F_x}{F_z}$, $\frac{M_x}{F_z}$ and $\frac{F_y}{F_z}$, we can obtain three kinds of jamming diagrams about three dimensional dual peg-in-hole problems (Fig.7):

(a) $\frac{M_y}{DF_z}\propto\frac{F_x}{F_z}$; (b) $\frac{M_x}{DF_z}\propto\frac{F_y}{F_z}$, $\alpha_1\in[0^\circ\ \ 90^\circ]$, $\alpha_3\in[0^\circ\ \ 90^\circ]$, $\alpha_2\in[180^\circ\ \ 270^\circ]$, $\alpha_4\in[180^\circ\ \ 270^\circ]$; (c) $\frac{M_x}{DF_z}\propto\frac{F_y}{F_z}$, $\alpha_1\in[270^\circ\ \ 360^\circ]$, $\alpha_3\in[270^\circ\ \ 360^\circ]$, $\alpha_2\in[90^\circ\ \ 180^\circ]$, $\alpha_4\in[90^\circ\ \ 180^\circ]$. Here $\frac{M_y}{DF_z}\propto\frac{F_x}{F_z}$ represents the linear relation between $\frac{M_y}{DF_z}$ and $\frac{F_x}{F_z}$, and $\frac{M_x}{DF_z}\propto\frac{F_y}{F_z}$ represents the linear relation between $\frac{M_x}{DF_z}$ and $\frac{F_y}{F_z}$.

There are some differences between the jamming diagram of a two dimensional dual peg-in-hole and that of a three dimensional dual peg-in-hole. In two dimensions, the jamming diagram only shows the linear relation between $\frac{M_x}{F_z}$ and $\frac{F_y}{F_z}$. The jamming diagram is not

relative to α_i and contact point positions (x_i y_i). It is only relative to μ, the insertion depth and the radii of peg and hole. In three dimensions, the linear relations between $\frac{M_y}{F_z}$ and $\frac{F_x}{F_z}$, $\frac{M_x}{F_z}$ and $\frac{F_y}{F_z}$ must be considered. The jamming diagrams are not only relative to μ, the insertion depth and the radii of peg and hole, but also relative to α_i and contact point positions (x_i y_i). Because the relation between $\frac{M_x}{F_z}$ and $\frac{F_y}{F_z}$ is relative to $sin\alpha_i$, according to the different range of α_i, the jamming diagrams can be discussed in Fig. 7(b) and Fig. 7(c).

In this section, the jamming diagrams of a three dimensional dual peg-in-hole are analyzed. The range of the jamming analysis is extended. Thus, the assembly process is analyzed in detail. We can know the whole assembly process of the three dimensional dual peg-in-hole clearly.

Table 2 lists the force/moment conditions for 20 possible contact states. Fig. 7 shows the jamming diagrams of a three dimensional dual-peg problem with these contact states. When the force/moment conditions of all possible contact states of the three dimensional dual-peg insertion problem are plotted in force/moment space, the plots form a closed boundary which separates the force/moment space into two spaces; statically unstable space, and jamming space. The unstable space is the area enclosed by the boundary, and represents the conditions on the applied forces and moments that cause the pegs to unstably fall into the holes. The jamming space, on the other hand, is the area outside the boundary, and represents the force/moment conditions in which the pegs appear stuck in the holes because the applied forces and moments cannot overcome the net forces and moments due to frictional contact forces (Fig. 7). The jamming diagrams can supply us some successful insertion information. If the conditions on the applied forces and moments fall into the unstable space, the pegs can unstably fall into the holes and the continuity of insertion can be guaranteed. Since all 20 contact states cannot exist at a particular geometric condition, each jamming diagram representing a particular insertion problem is constructed from only some of the straight lines shown in Fig. 7. When the geometric dimensions and the insertion depth are known, some possible contact states can be formed and some possible jamming diagrams can be obtained (Fig. 8).

5.2 33 kinds of possible jamming diagrams

When the exact dimensions of the pegs and the insertion depth are known, possible contact states can be derived, and the jamming diagrams can be constructed. These jamming diagrams provide us with the information on how to apply forces and moments to the pegs in order to yield successful insertions. For three kinds of jamming diagrams in Fig. 7, each has 11 kinds of possible jamming diagrams. For example, for some particular insertion condition and geometric condition, the possible jamming diagrams can be constructed by joining four corresponding lines in Fig. 7 (a) forming an enclosed region (Fig. 8 a). There are several possible jamming diagrams that can be constructed in this way. In Fig. 8 a, vertexes of the quadrangle represent one-point contact states, such as (*l*-1), (*l*-2), (*r*-1), (*r*-2) in Fig. 8 (a-1). Lines of the quadrangle represent two-point contact states, such as (*l*-5), (*r*-5) in Fig. 8 (a-1).

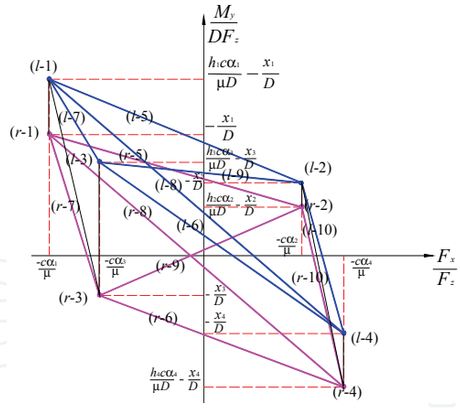

(a) $\frac{M_y}{DF_z} \propto \frac{F_x}{F_z}$

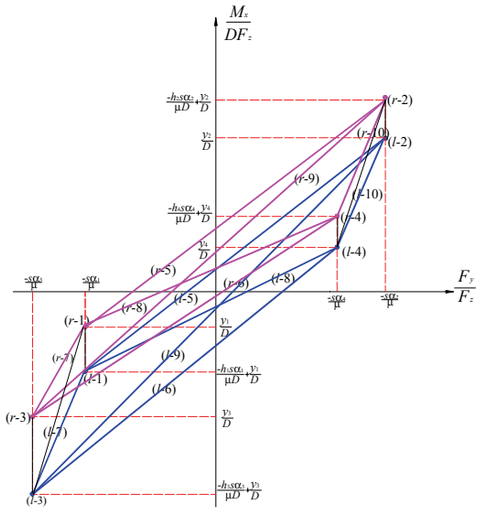

(b) $\frac{M_x}{DF_z} \propto \frac{F_y}{F_z}$, $\alpha_1 \in [0° \quad 90°], \alpha_3 \in [0° \quad 90°], \alpha_2 \in [180° \quad 270°], \alpha_4 \in [180° \quad 270°]$

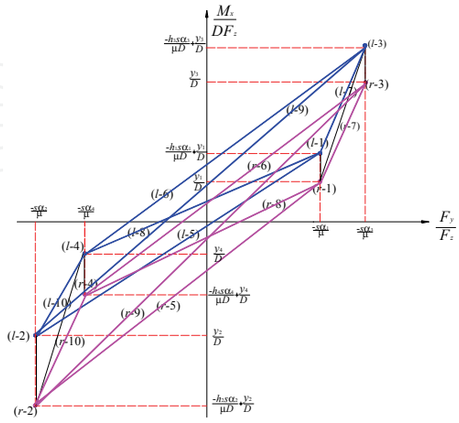

(c) $\frac{M_x}{DF_z} \propto \frac{F_y}{F_z}$, $\alpha_1 \in [270° \quad 360°], \alpha_3 \in [270° \quad 360°], \alpha_2 \in [90° \quad 180°], \alpha_4 \in [90° \quad 180°]$

Fig. 7. Jamming diagrams.

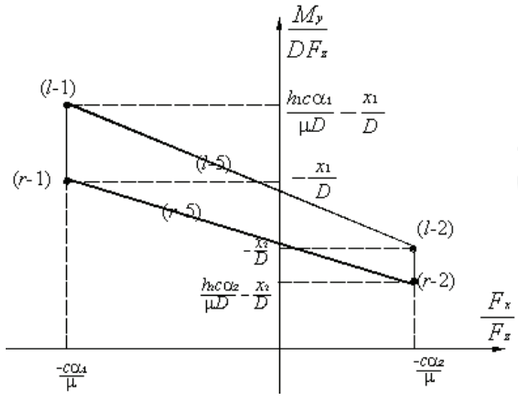

(a-1)

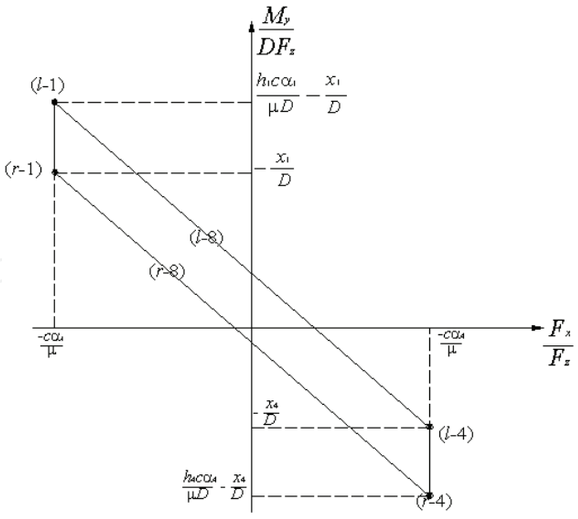

(a-2)

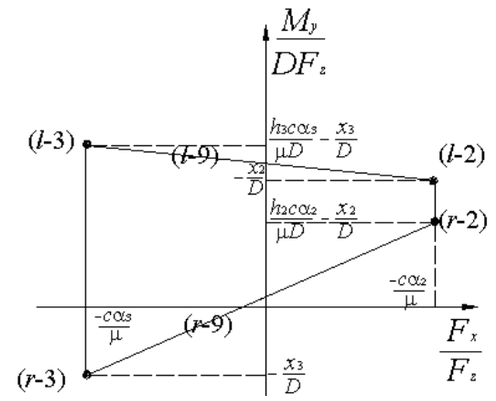

(a-3)

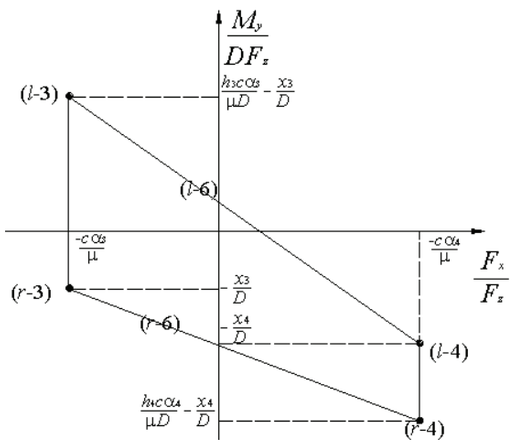

(a-4)

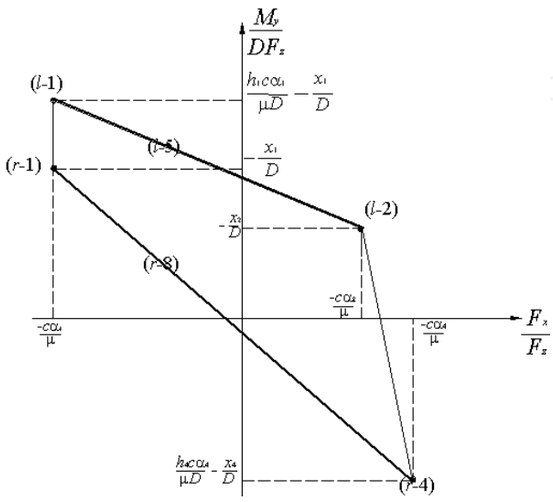

(a-5)

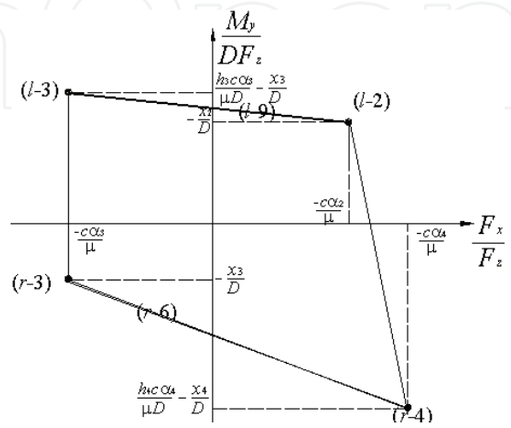

(a-6)

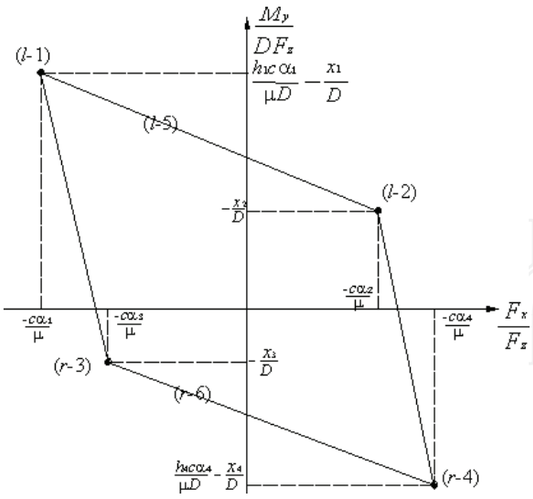

(a-7)

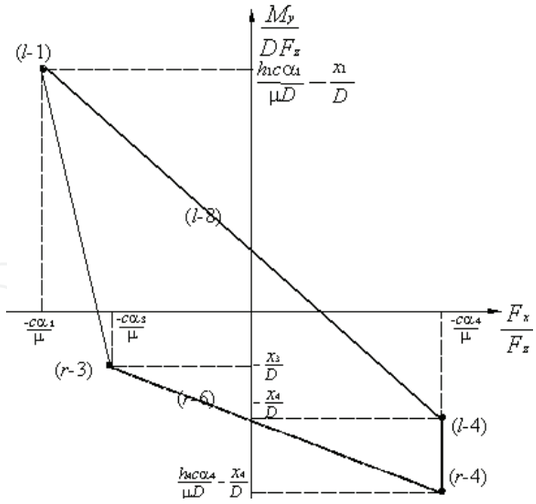

(a-8)

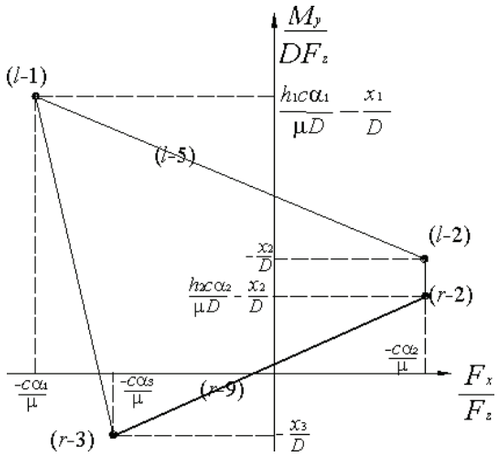

(a-9)

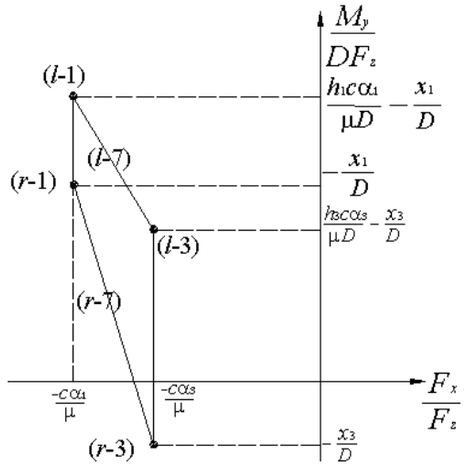

(a-10)

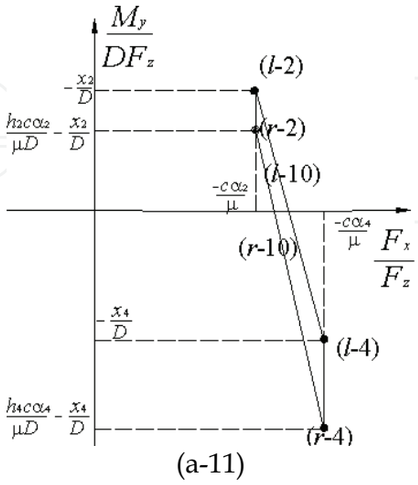

(a-11)

(a) Possible jamming diagrams ($\frac{M_y}{DF_z} \propto \frac{F_x}{F_z}$).

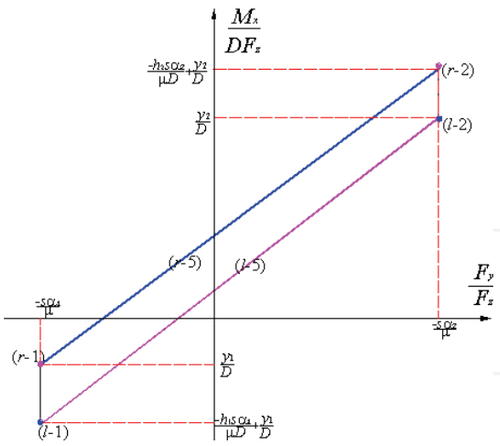

(b-1)

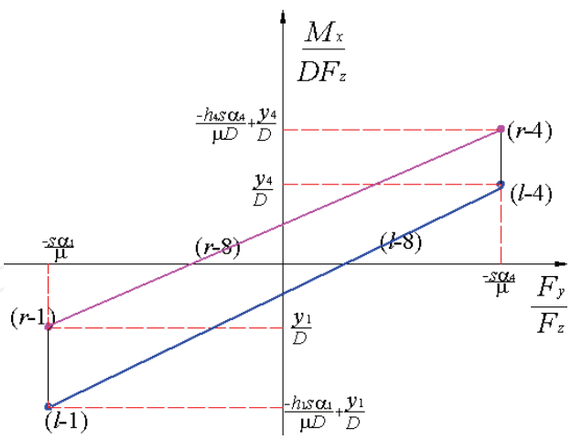

(b-2)

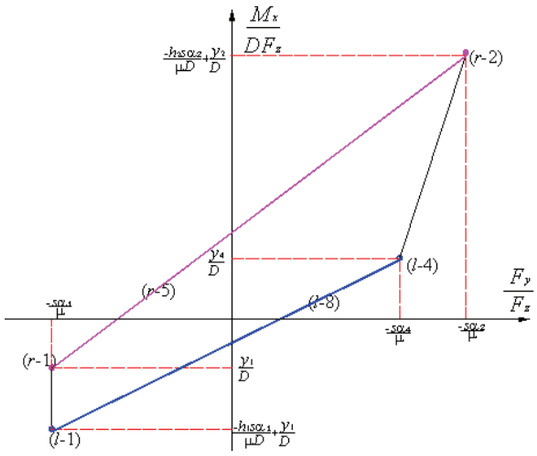

(b-3)

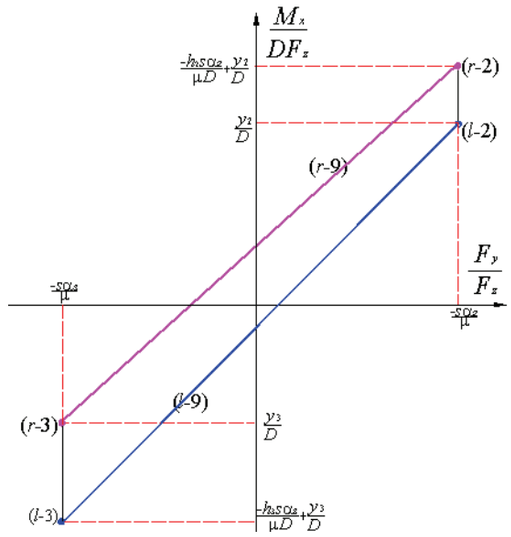

(b-4)

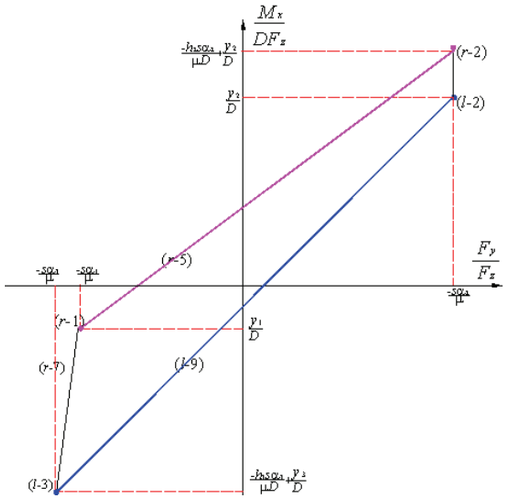

(b-5)

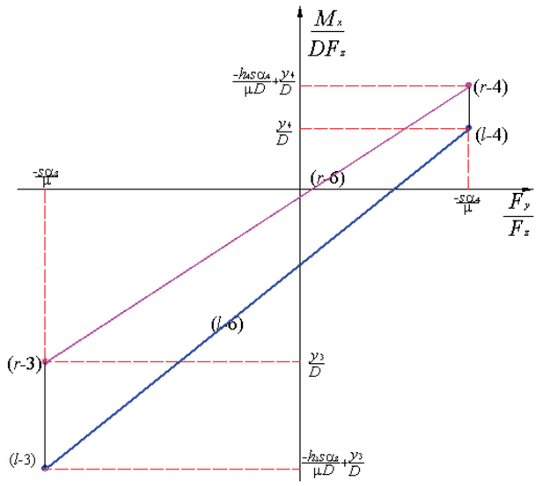

(b-6)

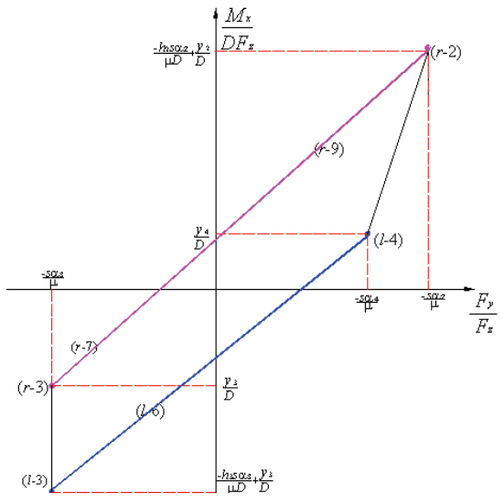

(b-7)

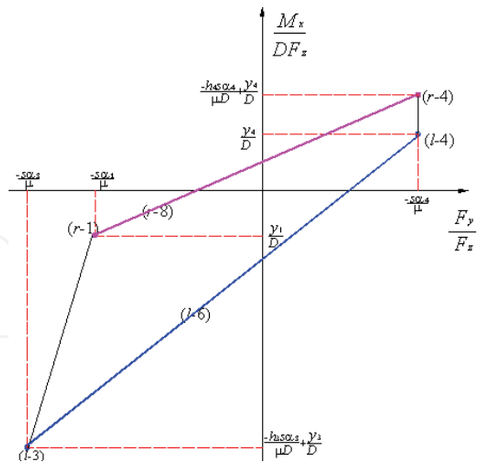

(b-8)

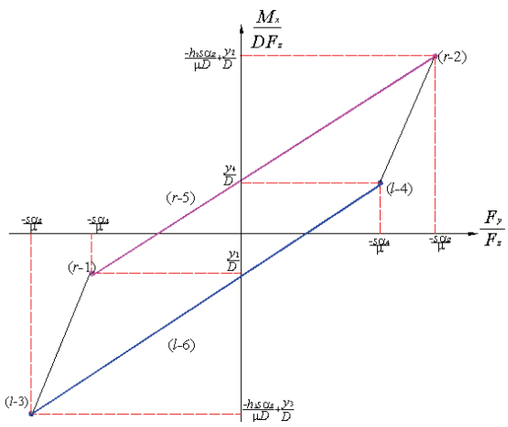

(b-9)

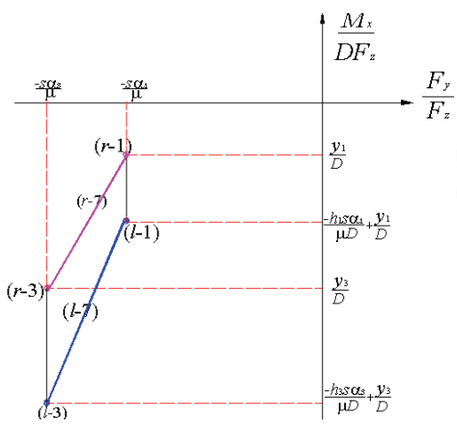

(b-10)

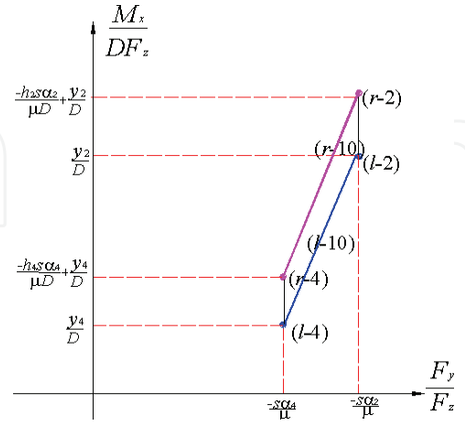

(b-11)

(b) Possible jamming diagrams: $\frac{M_x}{DF_z} \propto \frac{F_y}{F_z}$, $\alpha_1 \in [0° \quad 90°]$, $\alpha_3 \in [0° \quad 90°]$, $\alpha_2 \in [180° \quad 270°]$, $\alpha_4 \in [180° \quad 270°]$

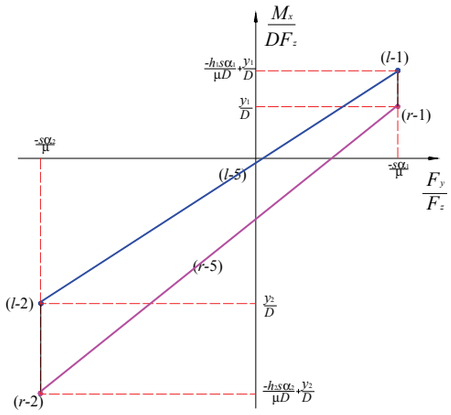

c-1

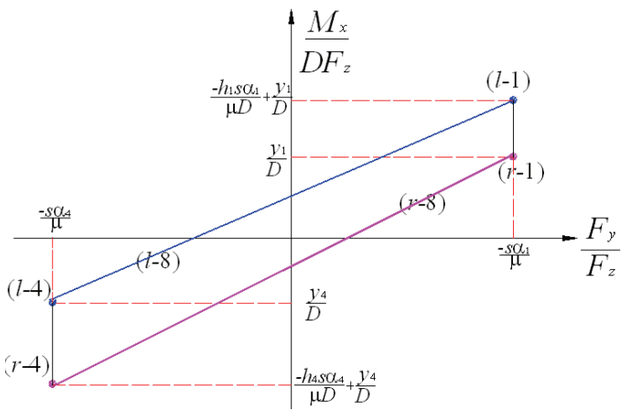

c-2

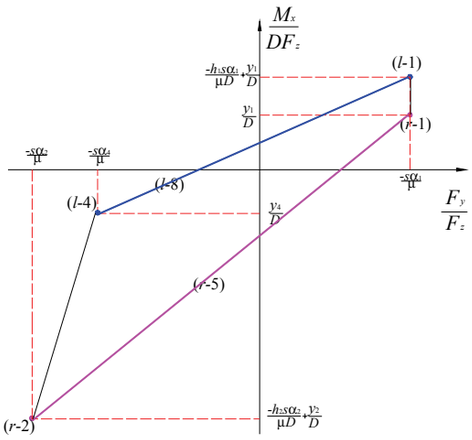

c-3

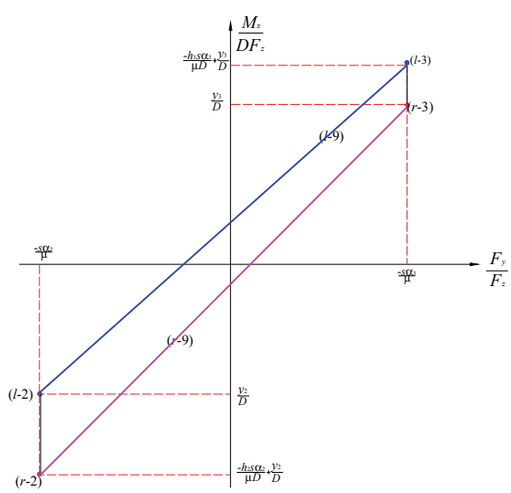

c-4

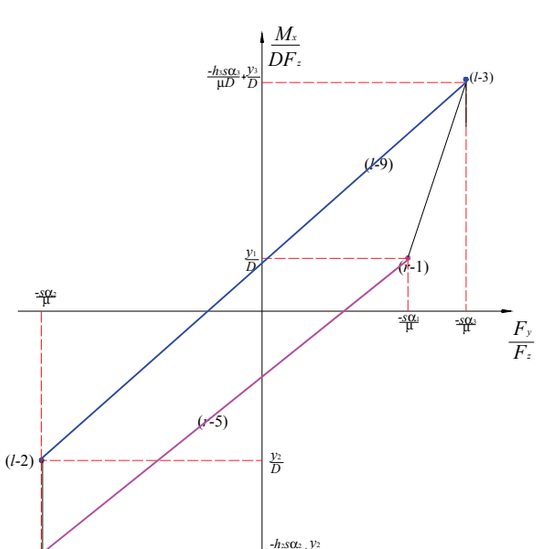

c-5

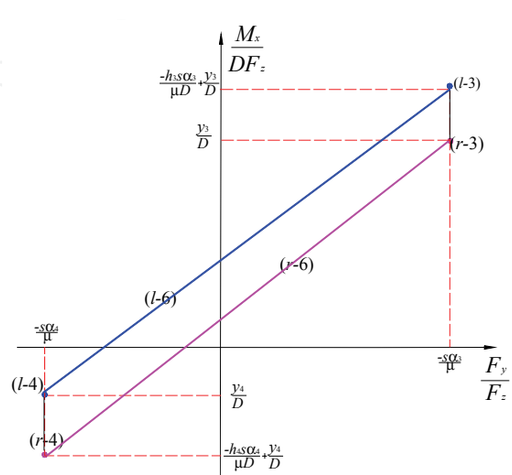

c-6

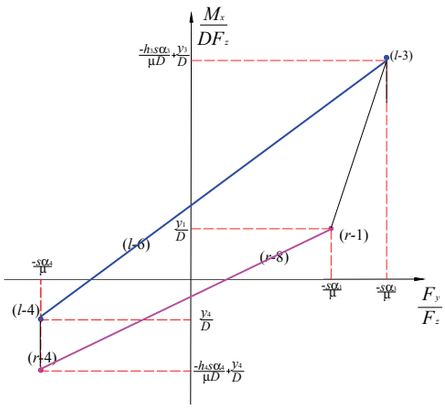

c-7

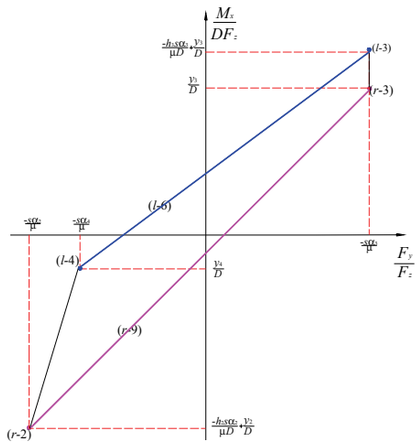

c-8

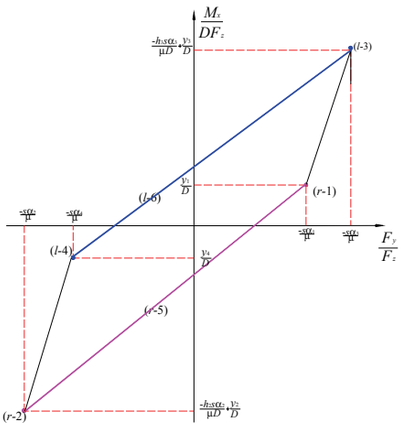

c-9

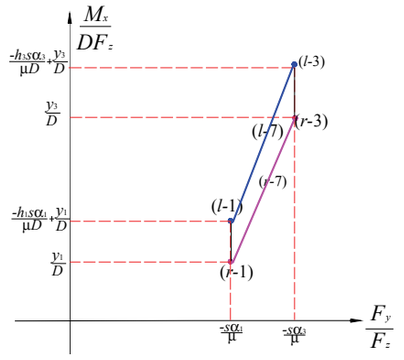

c-10

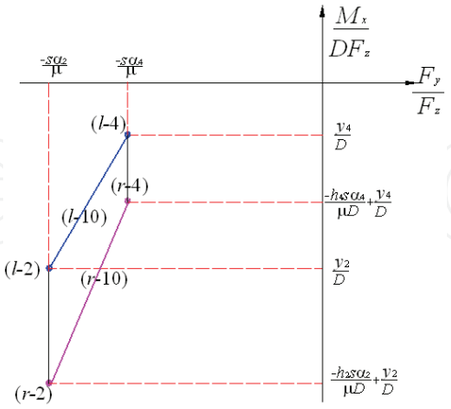

c-11

(c) Possible jamming diagrams: $\frac{M_y}{DF_z} \propto \frac{F_x}{F_z}$, $\alpha_1 \in [270° \quad 360°]$, $\alpha_3 \in [270° \quad 360°]$, $\alpha_2 \in [90° \quad 180°]$, $\alpha_4 \in [90° \quad 180°]$

Fig. 8. Possible jamming diagrams.

In two dimensions, there are only 9 kinds of jamming diagrams, which are static and relative to μ, the insertion depth and the radii of peg and hole. In three dimensions, there are 33 kinds of jamming diagrams, which are relative to not only μ, the insertion depth and the radii of peg and hole, but also α_l and contact point positions (x_i y_i). They are dynamic. The quadrangles are more complicated than those in two dimensions. In three dimensions, the possible jamming diagrams, such as Fig.8 (a-10) and Fig.8 (a-11), may appear. Fig.8 (a-10) shows the possible jamming diagram of left-contact. Fig.8 (a-11) shows the possible jamming diagram of right-contact.

The 33 kinds of possible jamming diagrams in Fig.8 may be interpreted as follows. The vertical lines in the diagrams describe line contact states. Combinations of F_x, F_z, and M_y falling on the parallelograms'edges describe equilibrium sliding in. Outside the parallelogram lie combinations which jam the dual-peg, either in one- or two-point contact. Inside, the dual-peg is in disequilibrium sliding or falling in.

6. Conclusions

In order to know the assembly process of a dual peg-in-hole and plan an insertion strategy in detail, it is important to analyze the dual peg-in-hole in three dimensions. In this paper, the assembly contact and jamming of a dual peg-in-hole in three dimensions are analyzed in detail. Firstly, 20 contact states of the three dimensional dual-peg are enumerated and geometric conditions are derived. Secondly, the contact forces are described by the screw theory in three dimensions. With the static equilibrium equations, the relationship between forces and moments for maintaining each contact state is derived. Thirdly, the jamming diagrams of the three dimensional dual peg-in-hole are presented. Different peg and hole geometry, and different insertion depth may yield different jamming diagrams. 33 different types of possible jamming diagrams for each jamming diagram are identified. These jamming diagrams can be used to plan fine motion strategies for successful insertions. In addition, they also show that the assembly process in six degrees of freedom is more complicated than that for planar motion. The above analyses are the theoretical bases for multiple peg-in-hole insertion. It is one most significant advance in robotic assembly.

7. References

Arai T., et al (1997). Hole search planning for peg-in-hole problem, *Manufacturing Systems*, 26(2), 1997, 119-124, ISSN: 0748-948X.

Fei Y.Q. and Zhao X.F.(2003). An assembly process modeling and analysis for robotic multiple peg-in-hole, *Journal of Intelligent and Robotic Systems*, 36(2), 2003, 175-189, ISSN: 0921-0296.

McCarragher B.J. and Asada H.(1995). The discrete event control of robotic assembly tasks, *Journal of Dynamic System, Measurement and Control*, 117(3), 1995, 384-393, ISSN: 0022-0434 .

Rossitza S. and Damel B.(1998). Three-dimensional simulation of accommodation, *Assembly Automation*, 18(4), 1998, 291-301, ISSN: 0144-5154.

Simunovic S.N.(1972). Force information in assembly process, *Proc. Of the 5th Int'l Symposium on Industrial Robots*, pp. 113-126, Chicago, Illinois, 1972, IIT Research Institute Chicago, Illinois.

Sturges R.H.(1988). A three-dimensional assembly task quantification with application to machine dexterity, *The Int. Journal of Robotics Research*, 7(1), 1988, 34-78, ISSN: 0278-3649.

Sturges R.H. and Laowattana S.(1996). Virtual wedging in three-dimensional peg insertion tasks, *Journal of Mechanical Design*, 118, 1996, 99-105, ISSN: 1050-0472.

Sturges R.H. and Laowattana S.(1996). Design of an orthogonal compliance for polygonal peg insertion, *Journal of Mechanical Design*, 118, 1996, 106-114, ISSN: 1050-0472.

Sturges R.H. and Sathirakul K.(1996). Modeling multiple peg-in-hole insertion tasks, *Proc. of the Japan/USA Symposium on Flexible Automation*, pp.819-821, Conference code: 46109, Boston, MA, USA, July 7-10, 1996, ASME.

Sathirakul K. and Sturges R.H.(1998). Jamming conditions for multiple peg-in-hole assemblies, *Robotica*, 16, 1998, 329-345, ISSN: 0263-5747.

Tsaprounis C.J. and Aspragathos N.(1998). Contact point identification in robot assembly strategies under uncertainty, *Robotica*, 16, 1998, 1679-690, ISSN: 0263-5747.

Whitney D.E.(1982). Quasi-static assembly of compliantly supported rigid parts, *ASME Journal of Dynamic Systems, Measurement, and Control*, 104, 1982, 65-77, ISSN: 0022-0434.

Xiao J. (1993). Automatic determination of topological containts in the presence of sensing uncertainties, *Proc. of IEEE Int. Conf. on Robotics and Automation*, pp.65-70, ISBN: 0-8186-3450-2, Atlanta, GA, USA, May 2-6, 1993, IEEE.

Xiao J.and Ji Xuerong (2001). Automatic generation of high-level contact state space, *The Int. Journal of Robotics Research*, 20(7), 2001, 584-606, ISSN: 1050-0472.

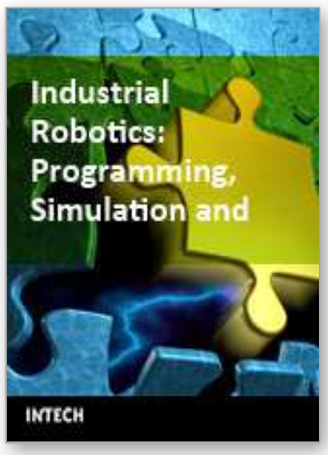

Industrial Robotics: Programming, Simulation and Applications

Edited by Low Kin Huat

ISBN 3-86611-286-6

Hard cover, 702 pages

Publisher Pro Literatur Verlag, Germany / ARS, Austria

Published online 01, December, 2006

Published in print edition December, 2006

This book covers a wide range of topics relating to advanced industrial robotics, sensors and automation technologies. Although being highly technical and complex in nature, the papers presented in this book represent some of the latest cutting edge technologies and advancements in industrial robotics technology. This book covers topics such as networking, properties of manipulators, forward and inverse robot arm kinematics, motion path-planning, machine vision and many other practical topics too numerous to list here. The authors and editor of this book wish to inspire people, especially young ones, to get involved with robotic and mechatronic engineering technology and to develop new and exciting practical applications, perhaps using the ideas and concepts presented herein.

InTech Europe
University Campus STeP Ri
Slavka Krautzeka 83/A
51000 Rijeka, Croatia
Phone: +385 (51) 770 447
Fax: +385 (51) 686 166
www.intechopen.com

InTech China
Unit 405, Office Block, Hotel Equatorial Shanghai
No.65, Yan An Road (West), Shanghai, 200040, China
中国上海市延安西路65号上海国际贵都大饭店办公楼405单元
Phone: +86-21-62489820
Fax: +86-21-62489821

IntechOpen